The Radiative Effect of Aerosols in the Earth's Atmosphere

WEI-CHYUNG WANG[1]

Goddard Institute for Space Studies, NASA, New York, N. Y. 10025

GERALD A. DOMOTO

Mechanical Engineering Department, Columbia University, New York, N. Y.

(Manuscript received 11 March 1974)

ABSTRACT

A modified two-flux approximation is employed to compute the transfer of radiation in a finite, inhomogeneous, turbid atmosphere. A perturbation technique is developed to allow the treatment of non-gray gaseous absorption with multiple scattering. The perturbation method, which employs a backscatter factor as a parameter, can be used with anisotropic particle scattering as well as Rayleigh scattering.

This method is used to study the effect of aerosols on radiative solar heating and infrared cooling as well as the radiative-convective temperature distribution in the earth's atmosphere. It is found that the effect of aerosols in the infrared cannot be neglected; while in the visible, the effect can be the same order as that due to absorption by water vapor. For a high surface albedo (>0.30) heating of the earth–atmosphere system results due to the presence of aerosols. The aerosols also reduce the amount of convection needed to maintain a stable atmosphere. For the case of a dense haze a temperature inversion is found to exist close to the ground.

1. Introduction

Because of the complexity of molecular absorption, the main difficulty in the analysis of radiation heat transfer in an emitting, absorbing and multiple scattering medium is the necessity for solving the equation of radiative transfer at a sufficient number of frequencies to define the line shape of the spectra. But even if the detailed absorption coefficients were known, the disadvantage with straightforward application of popular methods (Twomey *et al.*, 1966; van de Hulst, 1963; van de Hulst and Grossman, 1968; Kattawar and Plass, 1968; Grant and Hunt, 1968; Hansen, 1969) for multiple scattering is that the calculation would be very time consuming to cover the complete spectrum. Therefore, line-by-line calculation is usually adopted only as a method for checking the accuracy of approximate methods. In general, most calculations are based on approximate treatments of various aspects of radiative transfer theory.

There are numerous approximate methods to solve the radiative transfer equation in a plane-parallel turbid atmosphere (Schuster, 1905; Schwarzchild, 1906; Chu and Churchill, 1955; Pitts, 1954; Chandrasekhar, 1960; Romanova, 1962; Sagan and Pollack, 1967; Potter, 1970; Canosa and Penafiel, 1973; Uesugi and Irvine, 1969). But the lack of monochromatic absorption coefficients makes it necessary to use laboratory transmission functions, which are averaged over finite frequency intervals. Consequently, it is desirable to employ solutions of the transfer equation which have a form appropriate for using transmission function data.

In recent years, the large-scale increase of pollutants in the earth's atmosphere due to human activity has caused serious concern. The general aspects of climate change are discussed in Landsberg (1970) and SCEP (1970). Several authors (e.g., McCormick and Ludwig, 1967; Charlson and Pilat, 1969; Rasool and Schneider, 1971; Mitchell, 1971; Yamamoto and Tanaka, 1972; Braslau and Dave, 1973) have suggested that the increase of aerosols could either cause cooling or heating of the earth-atmosphere system, depending on the relative magnitude of the aerosol absorption and backscattering coefficients. But most work has emphasized the effect of aerosols on the transfer of solar radiation and neglected their effect in the infrared.

The purpose of this research is twofold: 1) to investigate an approximate method for solution of anisotropic particle scattering with non-gray gaseous absorption; and 2) to study the effect of aerosols on radiative solar heating and infrared cooling as well as on the radiative-convective temperature distribution of the earth's atmosphere.

[1] This paper is based on the author's doctoral dissertation presented to the Mechanical Engineering Department, Columbia University.

2. Analysis

The basic radiative transfer equation is

$$\mu\frac{\partial I_\nu}{\partial \tau_\nu}=-I_\nu(\tau_\nu)+(1-a_\nu)I_{b\nu}+\frac{a_\nu}{2}\int_{-1}^{1}I_\nu(\tau_\nu,\mu')P(\tau_\nu,\mu,\mu')d\mu', \quad (1)$$

where τ_ν is the optical depth, θ the zenith angle ($\mu=\cos\theta$), a_ν the single-scattering albedo ($a_\nu=k_{\nu s}/k_{\nu t}$, with subscripts s, t and a denoting scattering, extinction and absorption respectively), and $k_{\nu t}=k_{\nu s}+k_{\nu a}$; $I_{b\nu}$ is the spectral Planck function corresponding to local temperature under the condition of local thermodynamic equilibrium; and $P(\tau_\nu,\mu,\mu')$ is the scattering phase function. The phase function satisfies the normalization condition

$$\tfrac{1}{2}\int_{-1}^{1}P(\tau_\nu,\alpha)d(\cos\alpha)=1. \quad (2a)$$

The first moment of the phase function, defined as the asymmetry factor,

$$\langle\cos\alpha\rangle=\tfrac{1}{2}\int_{-1}^{1}P(\tau_\nu,\alpha)\cos\alpha d(\cos\alpha), \quad (2b)$$

characterizes the relative importance of forward-to-backward scattering.

The boundary conditions can be written as

$$I_\nu(\tau_{0\nu},\mu)=S_\nu\delta[\mu-(-\mu_0)], \quad \mu<0, \quad (3a)$$

$$I_\nu(0,\mu)=e_\nu I_{B\nu}+\rho_\nu I_\nu(0,-\mu), \quad \mu>0, \quad (3b)$$

where $2\pi\mu S_\nu$ is the solar irradiance perpendicular to the upper free surface ($\tau_\nu=\tau_{0\nu}$); $I_{B\nu}$ is the spectral Planck function at the lower surface ($\tau_\nu=0$) which has monochromatic diffuse emissivity e_ν and reflectivity ρ_ν; and $\delta[\ ]$ denotes the Dirac delta function.

Following Chandrasekhar (1960) with Legendre polynomial expansion of the phase function, application of moments, and the division of radiation field into two streams according to Gaussian quadrature, we obtain two linear coupled differential equations governing the *globally averaged* diffuse field (integrated over μ_0) as derived in Wang (1973):

$$\frac{1}{\sqrt{3}}\frac{dF_\nu^+}{d\tau_\nu}=(a_\nu-ba_\nu-1)F_\nu^++ba_\nu F_\nu^-+(1-a_\nu)I_{b\nu}+(1-b)a_\nu G_\nu\exp(-\sqrt{3}\tau_\nu)+\frac{a_\nu}{2}S_\nu b\exp[-\sqrt{3}(\tau_{0\nu}-\tau_\nu)], \quad (4a)$$

$$-\frac{1}{\sqrt{3}}\frac{dF_\nu^-}{d\tau_\nu}=(a_\nu-ba_\nu-1)F_\nu^-+ba_\nu F_\nu^++(1-a_\nu)I_{b\nu}+ba_\nu G_\nu\exp(-\sqrt{3}\tau_\nu)+\frac{a_\nu}{2}S_\nu(1-b)\exp[-\sqrt{3}(\tau_{0\nu}-\tau_\nu)], \quad (4b)$$

$$G_\nu=e_\nu I_{B\nu}+\rho_\nu\frac{S_\nu}{2}\exp(-\sqrt{3}\tau_{0\nu})+\rho_\nu F_\nu^-(0), \quad (4c)$$

where b is the backscatter factor defined as

$$2b(\tau_\nu)=1-\langle\cos\alpha\rangle. \quad (5)$$

The boundary conditions are

$$\left.\begin{aligned}F_\nu^+(0)&=0\\F_\nu^-(\tau_{0\nu})&=0\end{aligned}\right\}, \quad (6)$$

and the total flux, which is the sum of direct unscattered flux and the diffuse flux, is

$$F_\nu(\tau_\nu)=2\pi\int_{-1}^{1}I_\nu(\tau_\nu,\mu)\mu d\mu=\frac{2\pi}{\sqrt{3}}[F_\nu^+(\tau_\nu)-F_\nu^-(\tau_\nu)]+\frac{2\pi}{\sqrt{3}}e_\nu I_{B\nu}\exp(-\sqrt{3}\tau_\nu)-\frac{2\pi}{\sqrt{3}}\frac{S_\nu}{2}\exp[-\sqrt{3}(\tau_{0\nu}-\tau_\nu)]+\frac{2\pi}{\sqrt{3}}\rho_\nu\left[\frac{S_\nu}{2}\exp(-\sqrt{3}\tau_{0\nu})+F_\nu^-(0)\right]\times\exp(-\sqrt{3}\tau_\nu). \quad (7)$$

From (7), we can see that the total flux is amplified by a factor of $2/\sqrt{3}$ due to *Gaussian division* of the radiation field. Therefore, we redefine $I_{b\nu}$, $I_{B\nu}$, S_ν such that this factor is cancelled out in order to have energy conserved.

Sagan and Pollack (1967) used the same equations as (4) to study the clouds of Venus. They correlated the backscatter factor b to the asymmetry factor $\langle\cos\alpha\rangle$ as in (5) based on a comparison of transmitted flux with the exact solution of the phase function $1+3\langle\cos\alpha\rangle\cos\alpha$.

Tremendous computing time would be required in order to carry out the numerical integration of (4) even if the necessary detailed knowledge of molecular spectra (line intensity, shape and position) were available. Furthermore, high-resolution data of the atmospheric gases in the infrared are not available. Instead, one measures the transmittance averaged over the interval $\Delta\nu_j$ for a path length X_z (mass or pressure

path length) as

$$\bar{T}^g_{ja}=\frac{1}{\Delta\nu_j}\int_{\Delta\nu_j}\exp(-k^g_{\nu a}X_z)d\nu, \tag{8}$$

where superscripts p and g denote particles and gases, respectively, and $\Delta\nu_j$ is the frequency interval centered at ν_j. Therefore, the single-scatter albedo a_ν is not known explicitly. We proceed to use a perturbation technique such that (4) is decoupled and the solutions are in the form of expression (8) which can be obtained from laboratory measurements.

Let the normalized molecular and particle size distribution functions $n^g(r)$ and $n^p(r)$, where r is the radius of particles or molecules, be independent of z, i.e., constant at all altitudes. Then the phase function for the mixtures can be expressed as

$$P(z,\alpha)=\frac{k^p_{\nu s}(z)P^p(\alpha)+k^g_{\nu s}(z)P^g(\alpha)}{k^p_{\nu s}(z)+k^g_{\nu s}(z)}$$
$$=r^p_{\nu s}(z)P^p(\alpha)+r^g_{\nu s}(z)P^g(\alpha), \tag{9}$$

under the condition that radiation is scattered independently by gas molecules and particles; $P^p(\alpha)$ and $P^g(\alpha)$ are normalized phase functions for particles and molecules, respectively.

From (2b) and (5), we have

$$\langle\cos\alpha\rangle=r^p_{\nu s}(z)\langle\cos\alpha\rangle^p+r^g_{\nu s}(z)\langle\cos\alpha\rangle^g, \tag{10}$$

$$b=r^p_{\nu s}(z)b^p+r^g_{\nu s}(z)b^g, \tag{11}$$

where $\langle\cos\alpha\rangle^p$ and $\langle\cos\alpha\rangle^g$ are the asymmetry factors for particles and molecules, respectively. Both b^p and b^g are independent of z; b^g is 0.5 for Rayleigh scattering; b^p is around 0.15 for aerosols and hazes in the earth's atmosphere. A double expansion of the fluxes about these two parameters results in

$$F_\nu^+(\tau_\nu)=\sum_{m=0}\sum_{n=0}F^+_{\nu m,n}(\tau_\nu)(b^g)^m(b^p)^n, \tag{12a}$$

$$F_\nu^-(\tau_\nu)=\sum_{m=0}\sum_{n=0}F^-_{\nu m,n}(\tau_\nu)(b^g)^m(b^p)^n. \tag{12b}$$

Physically, the zeroth-order flux is that for a totally forward scattering system, while the higher order solutions are the corrections for neglecting the backscatter fraction.

Substituting (12) into (4) and collecting terms, we have the following perturbation equations and solutions:

a. Zeroth-order equations ($m=0$, $n=0$)

$$\frac{1}{\sqrt{3}}\frac{dF^+_{\nu 0,0}}{d\tau_\nu}=-(1-a_\nu)F^+_{\nu 0,0}$$
$$+a_\nu G_{\nu 0,0}\exp(-\sqrt{3}\tau_\nu)+(1-a_\nu)I_{b\nu}, \tag{13a}$$

$$-\frac{1}{\sqrt{3}}\frac{dF^-_{\nu 0,0}}{d\tau_\nu}=-(1-a_\nu)F^-_{\nu 0,0}$$
$$+\frac{a_\nu}{2}S_\nu\exp[-\sqrt{3}(\tau_{0\nu}-\tau_\nu)]$$
$$+(1-a_\nu)I_{b\nu}, \tag{13b}$$

$$G_{\nu 0,0}=e_\nu I_{B\nu}+\rho_\nu\frac{S_\nu}{2}\exp(-\sqrt{3}\tau_{0\nu})+\rho_\nu F^-_{\nu 0,0}(0). \tag{13c}$$

The boundary conditions are

$$\left.\begin{aligned}F^+_{\nu 0,0}(0)&=0\\ F^-_{\nu 0,0}(\tau_{0\nu})&=0\end{aligned}\right\}. \tag{13d}$$

Eqs. (13a, b) are decoupled and can be solved easily. The solutions in the integral form are

$$F^+_{\nu 0,0}(\tau_\nu)=\int_0^{\tau_\nu}I_{b\nu}(y)[T_{\nu a}(\tau_\nu,y)]_y dy$$
$$+G_{\nu 0,0}[T_{\nu a}(\tau_\nu,0)-T_\nu(\tau_\nu,0)], \tag{14a}$$

$$F^-_{\nu 0,0}(\tau_\nu)=-\int_{\tau_\nu}^{\tau_{0\nu}}I_{b\nu}(y)[T_{\nu a}(y,\tau_\nu)]_y dy$$
$$+\frac{S_\nu}{2}[T_{\nu a}(\tau_{0\nu},\tau_\nu)-T_\nu(\tau_{0\nu},\tau_\nu)], \tag{14b}$$

where

$$T_{\nu a}(x_1,x_2)=\exp\left[-\sqrt{3}\int_{x_2}^{x_1}(1-a_\nu)dx\right], \tag{14c}$$

$$T_\nu(x_1,x_2)=\exp[-\sqrt{3}(x_1-x_2)], \tag{14d}$$

$$[\ \ ]_y=\frac{d}{dy}[\ \ ]. \tag{14e}$$

b. First-order equations ($m=1$, $n=0$; $m=0$, $n=1$)

$$\frac{1}{\sqrt{3}}\frac{dF^+_{\nu 1,0}}{d\tau_\nu}=-(1-a_\nu)F^+_{\nu 1,0}+a_\nu r^g_{\nu s}(F^-_{\nu 0,0}-F^+_{\nu 0,0})$$
$$+a_\nu[\rho_\nu F^-_{\nu 1,0}(0)-r^g_{\nu s}G_{\nu 0,0}]\exp(-\sqrt{3}\tau_\nu)$$
$$+\frac{S_\nu}{2}a_\nu r^g_{\nu s}\exp[-\sqrt{3}(\tau_{0\nu}-\tau_\nu)], \tag{15a}$$

$$\frac{1}{\sqrt{3}}\frac{dF^-_{\nu 1,0}}{d\tau_\nu}=-(1-a_\nu)F^-_{\nu 1,0}+a_\nu r^g_{\nu s}(F^+_{\nu 0,0}-F^-_{\nu 0,0})$$
$$+a_\nu r^g_{\nu s}G_{\nu 0,0}\exp(-\sqrt{3}\tau_\nu)$$
$$-\frac{S_\nu}{2}a_\nu r^g_{\nu s}\exp[-\sqrt{3}(\tau_{0\nu}-\tau_\nu)]. \tag{15b}$$

The boundary conditions are

$$\left.\begin{aligned} F^{+}_{\nu 1,0}(0)&=0\\ F^{-}_{\nu 1,0}(\tau_{0\nu})&=0\end{aligned}\right\}. \tag{15c}$$

Substituting (14) into (15), we can solve for $F^{+}_{\nu 1,0}$, $F^{-}_{\nu 1,0}$ as

$$\begin{aligned} F^{+}_{\nu 1,0}(\tau_\nu)&=-\int_0^{\tau_\nu}\sqrt{3}a_\nu{}^g(y)T_{\nu a}(\tau_\nu,y)\int_y^{\tau_{0\nu}}I_{b\nu}(z)[T_{\nu a}(z,y)]_z dz dy\\ &\quad-\int_0^{\tau_\nu}\sqrt{3}a_\nu{}^g(y)\int_0^{y}I_{b\nu}(z)[T_{\nu a}(\tau_\nu,z)]_z dz dy\\ &\quad-G_{\nu 0,0}T_{\nu a}(\tau_\nu,0)\int_0^{\tau_\nu}\sqrt{3}a_\nu{}^g(y)dy\\ &\quad+\frac{S_\nu}{2}T_{\nu a}(\tau_{0\nu},\tau_\nu)\int_0^{\tau_\nu}\frac{a_\nu{}^g(y)}{[1-a_\nu(y)]}[T_{\nu a}(2\tau_\nu,2y)]_{2y}dy\\ &\quad+\rho_\nu F^{-}_{\nu 1,0}(0)[T_{\nu a}(\tau_\nu,0)-T_\nu(\tau_\nu,0)], \end{aligned} \tag{16a}$$

$$\begin{aligned} F^{-}_{\nu 1,0}(\tau_\nu)&=\int_{\tau_\nu}^{\tau_{0\nu}}\sqrt{3}a_\nu{}^g(y)T_{\nu a}(y,\tau_\nu)\int_0^{y}I_{b\nu}(z)[T_{\nu a}(y,z)]_z dz dy\\ &\quad+\int_{\tau_\nu}^{\tau_{0\nu}}\sqrt{3}a_\nu{}^g(y)\int_y^{\tau_{0\nu}}I_{b\nu}(z)[T_{\nu a}(z,\tau_\nu)]_z dz dy\\ &\quad-G_{\nu 0,0}T_{\nu a}(\tau_\nu,0)\int_{\tau_\nu}^{\tau_{0\nu}}\frac{a_\nu{}^g(y)}{[1-a_\nu(y)]}[T_{\nu a}(2y,2\tau_\nu)]_{2y}dy\\ &\quad-\frac{S_\nu}{2}T_{\nu a}(\tau_{0\nu},\tau_\nu)\int_{\tau_\nu}^{\tau_{0\nu}}\sqrt{3}a_\nu{}^g(y)dy, \end{aligned} \tag{16b}$$

where $a_\nu{}^u=a_\nu r^g_{\nu s}$; and for fluxes $F^{+}_{\nu 0,1}$, $F^{-}_{\nu 0,1}$, the equations are same except substituting $a_\nu{}^p$ for $a_\nu{}^u$.

c. Higher-order equations ($m\geq 2$, $n\geq 0$; $m\geq 0$, $n\geq 2$)

$$\begin{aligned} \frac{1}{\sqrt{3}}\frac{dF^{+}_{\nu m,n}}{d\tau_\nu}&=-(1-a_\nu)F^{+}_{\nu m,n}\\ &\quad+a_\nu[r^p_{\nu s}(F^{-}_{\nu m,n-1}-F^{+}_{\nu m,n-1})+r^g_{\nu s}(F^{-}_{\nu m-1,n}-F^{+}_{\nu m-1,n})]\\ &\quad-\rho_\nu a_\nu[r^p_{\nu s}F^{-}_{\nu m,n-1}(0)+r^g_{\nu s}F^{-}_{\nu m-1,n}(0)]\exp(-\sqrt{3}\tau_\nu)\\ &\quad+a_\nu\rho_\nu F^{-}_{\nu m,n}(0)\exp(-\sqrt{3}\tau_\nu), \end{aligned} \tag{17a}$$

$$\begin{aligned} -\frac{1}{\sqrt{3}}\frac{dF^{-}_{\nu m,n}}{d\tau_\nu}&=-(1-a_\nu)F^{-}_{\nu m,n}\\ &\quad+a_\nu[r^p_{\nu s}(F^{+}_{\nu m,n-1}-F^{-}_{\nu m,n-1})+r^g_{\nu s}(F^{+}_{\nu m-1,n}-F^{-}_{\nu m-1,n})]\\ &\quad+\rho_\nu a_\nu[r^p_{\nu s}F^{-}_{\nu m,n-1}(0)+r^g_{\nu s}F^{-}_{\nu m-1,n}(0)]\\ &\quad\times\exp(-\sqrt{3}\tau_\nu). \end{aligned} \tag{17b}$$

The boundary conditions are

$$\left.\begin{aligned} F^{+}_{\nu m,n}(0)&=0\\ F^{-}_{\nu m,n}(\tau_{0\nu})&=0\end{aligned}\right\}. \tag{17c}$$

The $(m+n)$th order solutions will involve $(m+n+1)$th integration over the path length. Although it is straightforward, we will not write down the lengthy solutions.

From (14), (16), and higher order perturbation equations, we can see that the solutions are in the form:

$$\text{(source function)}\ (\sqrt{3}b\tau_{\nu s})^n(T_{\nu a}),$$

where n is the order of the perturbation equation. The form is more or less like the Neumann series solution (Irvine, 1968), but converges much faster because of the smallness of b. A convergence problem arises with the perturbation solutions if the molecular and particle absorptions are small or zero ($T_{\nu a}\to 1$) for large optical thickness or $\sqrt{3}b\tau_{0\nu s}>1.0$. However, for a conservative scattering homogeneous layer, the exact solution of (4) is known. Therefore, knowing the zeroth- and first-order solutions, we put the solution in the approximate form:

$$\bar{F}_j=\frac{\bar{F}_{j0,0}}{1-\dfrac{b^u\bar{F}_{j1,0}+b^pF_{j0,1}}{\bar{F}_{j0,0}}}, \tag{18}$$

which matches exactly with the solutions of (4) for the conservative case as well as with the perturbation solution and the problem of divergence can be avoided. For the case $a_\nu\to 1$, expansion of both the exact solution of (4) and the approximation of (18) in $(1-a_\nu)$ yields agreement through terms of order $\tau_{0\nu}$. Therefore, the approximation (18) is strictly valid for $\sqrt{3}b\tau_{0\nu s}<1.0$, for all values of a_ν. But it may be applied for large values of $\sqrt{3}b\tau_{0\nu s}$ with reasonable results, especially for $a_\nu<0.4$ and >0.99, as will be shown.

In general, it is not possible to integrate (14)–(16) analytically. However, the atmosphere can be separated into a series of isothermal, homogeneous layers such that the properties are constant throughout each layer. In the following, we will first demonstrate the frequency integration using a band model for a homogeneous layer. The Curtis-Godson approximation is used to treat the inhomogeneous atmosphere.

Since the scattering coefficients and absorption coefficients of the scatterers are smooth functions of wavelength when averaged over size distribution, the only frequency integrations required are for the nongray gases involving transmittance and the reciprocal of the absorption coefficient as shown in (16) [e.g., the fourth term in (16a)]. For a homogeneous layer, the

term can be written as

$$\int_{\Delta\nu} a_\nu{}^g T_{\nu a}(\tau_{0\nu},\tau_\nu)\frac{[1-T_{\nu a}(2\tau_\nu,0)]}{2(1-a_\nu)}d\nu$$
$$=\int_{\Delta\nu}\sqrt{3}a_\nu{}^g\tau_\nu T_{\nu a}(\tau_{0\nu},\tau_\nu)\int_0^1 T_{\nu a}(2\tau_\nu x,0)dxd\nu,$$
$$=\sqrt{3}a_\nu{}^g\tau_\nu\int_0^1\int_{\Delta\nu} T_{\nu a}(\tau_{0\nu}+2\tau_\nu x,\tau_\nu)d\nu dx. \qquad (19)$$

Therefore, the solutions are in the form of (8) and the experimental data can be used by employing the band models. Within a small frequency interval in the band, the spectral emissivity of a non-gray gas can be represented with reasonable accuracy by theoretical models which could also correlate the experimental data. Extensive discussions of narrow or wide band models are to be found in the literature (Plass, 1963; Edwards and Menard, 1964; Tien, 1968; Goody, 1964; Malkmus, 1967). The choice of band models will depend on the properties of gases. For example, for the spectra of very complex molecules such as H_2O, CO_2 and other polyatomic molecules, the mean transmittivity (8) for the general statistical model with an exponential line intensity distribution can be written as (Tien, 1968; Goody, 1964)

$$\bar{T}_{ja}^g=\exp[-\beta X/(1+2X)^{\frac{1}{2}}], \qquad (20a)$$

where $\beta=2\pi\alpha_L/d$, $X=SX_z/(2\pi\alpha_L)$, and both the line spacing d and line intensity S are mean values over the band. For an exponential-tailed S^{-1} line intensity distribution, $\bar{T}_{ja}^g$ can be written as (Malkmus, 1967)

$$\bar{T}_{ja}^g=\exp\left\{-\frac{\beta_E}{\pi}[(1+2\pi X_E)^{\frac{1}{2}}-1]\right\}, \qquad (20b)$$

where $\beta_E=(\pi/4)\beta$, $X_E=(4/\pi)X$. For practical purposes, either of the line intensity distribution functions may be used because the difference between the absorption of different intensity distributions is small (Tien, *loc. cit.*).

Using the narrow band model of Malkmus, Domoto and Wang (1974) have obtained simple expressions of infrared transmittance, reflectance and emittance of water clouds typical of those in the earth's atmosphere.

The above-mentioned band radiation is limited to the case of a homogeneous gas layer. In general, nonhomogeneity results because of a distribution of local temperature, pressure and gas concentration (Tien, 1968; Goody, 1964). No exact solution can be obtained for the general problem of radiation heat transfer for an inhomogeneous path. The most useful and convenient among the approximate methods is the Curtis-Godson approximation, which replaces each inhomogeneous optical path with a hypothetical homogeneous path that has the same transmittance (Tien, *loc. cit.*). The approximation is exact at strong and weak line limits. The defined mean spectral emissivity is based on an equivalent homogeneous gas with mean line intensity to spacing ratio $\langle S/d\rangle$ and the mean Lorentz line half-width to spacing ratio $\langle\alpha_L/d\rangle$ given by (Tien)

$$\left\langle\frac{S}{d}\right\rangle X_z=\int_0^{X_z}\left(\frac{S}{d}\right)dz, \qquad (21a)$$

$$\left\langle\frac{S}{d}\right\rangle\left\langle\frac{\alpha_L}{d}\right\rangle X_z=\int_0^{X_z}\left(\frac{S}{d}\right)\left(\frac{\alpha_L}{d}\right)dx, \qquad (21b)$$

where $dx=\rho dz$, $X_z=\rho z$ and ρ is concentration. The terms inside the integral denote quantities based on homogeneous conditions corresponding to local temperature and effective pressure. Krakow *et al.* (1966) have compared the measured and computed (band model theory) transmittance. The error appeared to be due more to the band model theory than to the Curtis-Godson approximation.

Finally, we will discuss the accuracy of the present approximate method. Table 1 shows the comparison of transmittance of various approximate methods, the present matching approximation, and the exact solution for conservative isotropic scattering. The present approximation is better than other approximations in the range $0<\tau_0<2$. The small difference between Sagan and Pollack (1967) and the present method is due mainly to their using a constant different from $\sqrt{3}$.

For gray, nonconservative, anisotropic scattering, the asymmetry factor [$=0.8$ (typical value of clouds in the earth's atmosphere)] is chosen for comparison as shown in Figs. 1a and 1b. When $\tau_0=1.0$, the agreement is nearly perfect for all values of the single scattering albedo. Even for $\tau_0=10.0$, the approximation is in good agreement with the modified two-flux results for albedos <0.4 and >0.99.

TABLE 1. Comparison of transmittance of exact solution with various approximate methods and the present approximation for homogeneous, conservative, isotropic (or Rayleigh) scattering.

		Approximate solution			
Optical thickness	Exact solution*	Sagan and Pollack	Edding-ton	Two-flux method	Present method
0	1.0	1.0	1.0	1.0	1.0
0.05	0.95484	0.95868	0.96386	0.95238	0.95850
0.1	0.91566	0.92064	0.93023	0.90909	0.92030
0.15	0.88073	0.88550	0.89888	0.86957	0.88503
0.2	0.84906	0.85295	0.86957	0.83333	0.85237
0.5	0.7040	0.69881	0.72727	0.66667	0.69784
1.0	0.5534	0.53706	0.57143	0.5	0.53591
2.0	0.3900	0.36711	0.40	0.3333	0.36603
4.0	0.2459	0.22482	0.25	0.20	0.22401
10.0	0.1322	0.10395	0.11765	0.09091	0.10352
100.0	0.01315	0.01147	0.01316	0.00990	0.01142

* $\tau_0\leqslant 1.0$ (Chandrasekhar, 1960); $\tau_0>1.0$ (van de Hulst, 1964).

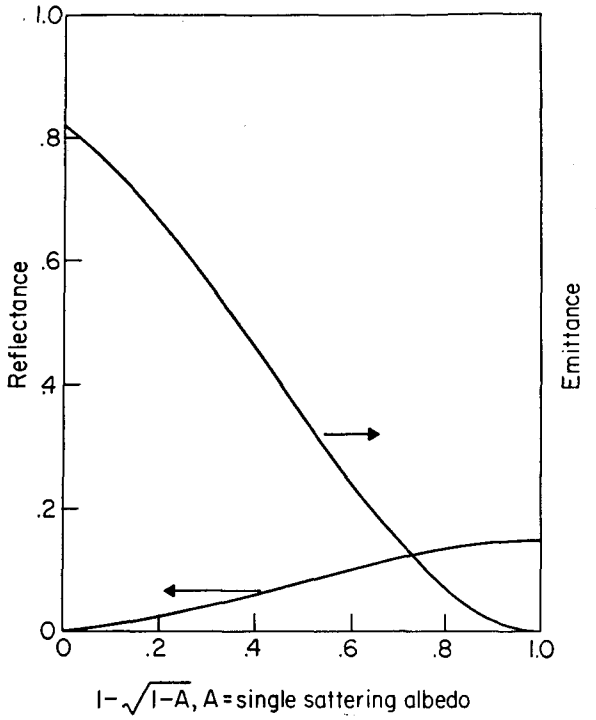

(a)

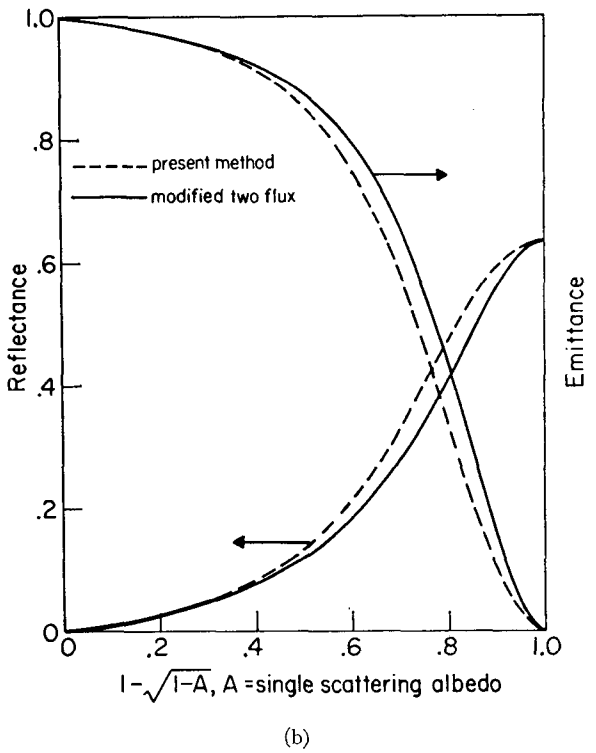

(b)

FIG. 1. Comparison of modified two-flux approximation and present method for an asymmetry factor of 0.8 and $\tau_0 = 1.0$ (a) and 10.0 (b).

The accuracy of the approximation in the non-gray case was examined by Domoto and Wang (1974). The frequency integration of the modified two-flux solutions was carried out using the absorption coefficient as the variable of integration together with an appropriate kernel function, which was obtained using the inverse Laplace transform of the transmission function based on the Malkmus model. Excellent agreement was observed between the approximation and the modified two-flux solutions.

3. Results and discussion

a. The atmospheric model

The atmosphere is divided into nine layers from the surface to an altitude of about 30 km according to the sigma coordinate system (Manabe and Strickler, 1964). The pressure levels which specify the atmospheric layers are 1010.00, 1000.99, 935.19, 819.50, 670.50, 505.00, 339.44, 190.50, 74.81 and 9.01 mb. The global-averaged values of the atmosphere shown in Table 2 are adopted for calculation.

In the infrared, the generalized absorption coefficients of Elsasser and Culbertson (1960)—which includes the rotation band and 6.3-μm band of water vapor, the 15-μm band of carbon dioxide, and the 9.0-, 9.6- and 14-μm bands of ozone—are fitted to Goody's random model. Zeroth- and first-order solutions are obtained by numerical integration of (14) and (16) over frequency from wavenumber 40 to 2240 cm^{-1} with an interval 10 cm^{-1} for overlapping regions and 40 cm^{-1} for non-overlapping regions.

The solar frequency spectrum 0.21–4.6 μm is divided into 61 spectral intervals and the solar energy based on 2 cal cm^{-2} min^{-1} and 6000K blackbody distribution is used. Only ozone absorption is considered in the visible and ultraviolet regions ($\lambda \leqslant 0.7$ μm) and the data tabulated in List (1968) are used. In the near infrared, water vapor and carbon dioxide are

TABLE 2. Model of the earth's atmosphere.

Surface	
Pressure P_0	1010 mb
Relative humidity	75%
Albedo ρ	0.105
Atmosphere	
Moist lapse rate γ	-6.5K km^{-1}
Tropopause	11 km
Cloud cover CLC	54%
Gaseous constituents	
Water vapor mixing ratio	
troposphere	$w_0(P/P_0)^3$ [Smith, 1966]
stratosphere	2.0E-6 gm gm^{-1}
Carbon dioxide	
constant mixing ratio	300 ppm
Ozone	Elterman (1968)

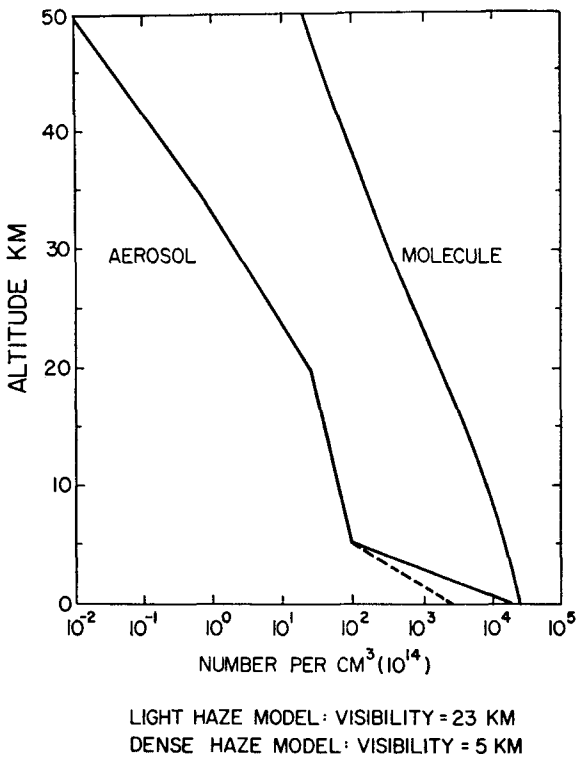

FIG. 2. Particle and molecular concentrations used in the present model.

treated. The transmission functions tabulated in the *Handbook of Geophysics*—which includes 0.94, 1.1, 1.38, 1.87, 2.7, 3.2 μm of water vapor and 1.4, 1.6, 2.0, 2.7, 4.3 μm of carbon dioxide—are fitted to Goody's random model.

Clouds play an important role in the radiation balance of the atmosphere. The presence of clouds considerably reduces the net radiation, while the atmospheric emission increases. The requirements on the knowledge of cloud heights, types, amounts, etc., for radiation calculations are formidable. However, for the purpose of simulating a relatively realistic atmosphere, we adopted a simple cloud model which involves a single cloud layer possessing mean spectral properties. The cloud albedo depends on the drop size distribution, water content, cloud thickness, etc. Previous measurements of the albedo of clouds given in the *Smithsonian Meteorological Tables* and Conover (1965) vary from 0.30 to 0.80. Robinson (1966) has estimated the mean cloud albedo around 0.5–0.55 based on energy balance. Throughout the solar spectrum a mean cloud albedo of 0.55 is used; this value is close to the mean value of low and middle cloud albedo used by Houghton (1954) [Angstrom (1962) also adopted this value from Houghton]. Neiburger (1949) observed the mean value of cloud absorptivity to lie between 0.05 to 0.09; Griggs (1968) estimated the value to be 0.04. In this calculation, absorption by cloud is neglected for $\lambda \leqslant 0.7$ μm, and whenever it is 0.02 in the near infrared; the value is smaller than 0.04 since, following Manabe and Strickler (1964), we assume the atmospheric water vapor absorbs radiant energy before it reaches the clouds. Following Robinson we adopted 54% as the normal cloud cover instead of 52% used by Houghton and Angstrom. The radiation which reaches the cloud base is assumed to be completely absorbed in the infrared and the energy re-emitted at the cloud temperature. So the effective cloud height is very important in determining the radiation escaping to space. No mean effective cloud height is cited in references [Rasool and Schneider (1971) used 5.0 km as an effective cloud height but with no reference]. In this calculation, we adopted 5.4 km (505 mb), chosen on the basis of several cloud calculations in the visible in order to give a reasonable global albedo due to clouds of around 0.25 as estimated by London (1957). The drastic heating or cooling due to the presence of clouds is smoothed out by the layer which contains the cloud.

The surface albedo is highly dependent upon the nature of the surface, ranging from 0.07 for oceans to 0.7 for old smooth snow-covered ground (List, 1968; Griggs, 1968). It is believed that the global mean surface albedo is between 0.1 and 0.2. Manabe and Strickler (1964) suggested the value of 0.102. We adopted the value of 0.105 which is the mean value over 30–40N (Sellers, 1965), where the annual mean value of radiation in believed balanced (Robinson, 1966).

As for aerosols, the scattering and absorption coefficients are taken from McClatchey *et al.* (1971) who describe a "clear" and a "hazy" atmosphere corresponding to a visibility of 23 and 5 km, respectively, at ground level. Fig. 2 shows the distributions of the number of particles for the two models as well as the molecules [taken from Elterman (1968)]. Most of the particles are confined to the lower 5 km. The size distribution function of the particles, $n^p(r)$ (shown in Table 3), is similar to the one suggested by Deirmendjian (1964) for continental haze. Figs. 3a and 3b show the optical thickness for the aerosol attenuation and molecular scattering in the solar and infrared regions. The Rayleigh scattering contribution is considered in the whole solar region but neglected in the infrared. The index of refraction [used by McClatchey

TABLE 3. Particle size distribution.

r (μm)	$n^p(r)$
$0.1 < r < 10$	$8.83(10r)^{-4}$
$0.02 < r < 0.1$	8.83
$r < 0.02$	0
$r > 10$	

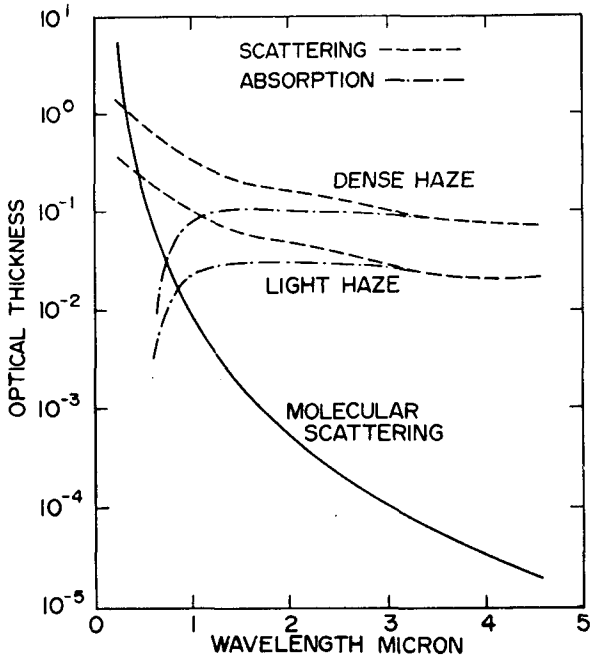

(a)

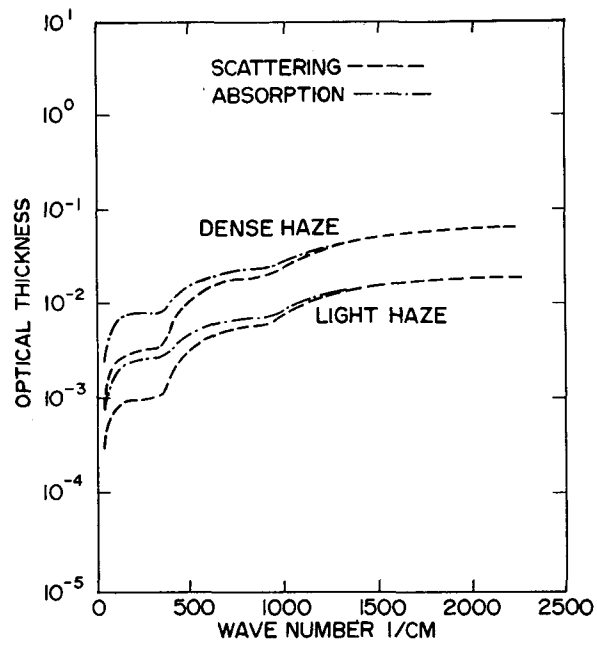

(b)

FIG. 3. Optical thickness versus frequency for aerosol attenuation and molecular scattering in the visible and near infrared (a) and the far infrared (b).

et al. (1971)] for aerosols is

$$n=\begin{cases}1.5+i0, & \lambda\leqslant 0.6\ \mu\text{m}\\ 1.5+i0.0714(\lambda-0.6), & 0.6\ \mu\text{m}<\lambda\leqslant 2\ \mu\text{m}\\ 1.5+i0.1, & \lambda>2\ \mu\text{m}\end{cases} \quad (22)$$

In the numerical calculations, three atmospheric models are used and categorized as follows:

Clear Model Atmosphere (CMA) which includes H_2O, CO_2 and O_3 gas absorbers and surface albedo of 0.105, if not specified explicitly.

Light Haze Atmosphere (LHA) which is CMA plus the "clear" aerosol model.

Dense Haze Atmosphere (DHA) which is CMA plus the "hazy" aerosol model. Rayleigh scattering (R) and clouds (C) are included if they are specified.

The infrared and solar heating rates, denoted by $(\partial T/\partial t)_{LW}$ and $(\partial T/\partial t)_{SW}$, respectively, are calculated according to

$$\frac{\partial T}{\partial t}=\frac{1}{\rho_a c_p}\frac{dF}{dz}, \quad (23)$$

where

$$F(z)=\int_\nu F_\nu(z)d\nu,$$

and c_p is the specific heat of air at constant pressure and ρ_a the density of air.

b. Solar radiation

First, the global albedo A_e (the backward scattered solar radiation divided by the incoming solar radiation) due to Rayleigh scattering, light or dense haze, and clouds is studied. Fig. 4 shows the global albedo of CMA, LHA and DHA for a surface albedo $\rho\leqslant 0.4$. About 10% of the solar energy is scattered back to space due to Rayleigh scattering and our adopted mean surface albedo of 0.105. The global albedo due to clouds only is 0.251. The computed albedo for CMA+R+C and surface albedo of 0.105 is 0.305 which agrees amazingly well with the observed value 0.30 (Vonder Haar and Suomi, 1971). The effect of aerosols, in general, is to decrease solar radiation reaching the earth's surface and increase the global albedo. Light haze and dense haze alone have backscatter values of 2.6 and 8.1%, respectively, for solar radiation; the effect is large because the aerosols affect the whole solar spectrum (see Fig. 3a), while Rayleigh scattering contributes only in the ultraviolet and visible which contains only $\sim\frac{1}{2}$ of the solar energy.

Table 4 shows the net incoming solar radiation at the earth's surface for various sky conditions. With respect to CMA, the LHA and DHA reduce this net flux by 6 and 19% for a cloudless atmosphere, and 10 and 35% for a cloudy atmosphere.

Furthermore, Table 5 shows the solar heating rate for various sky conditions. Dense haze has the same

TABLE 4. Net incoming solar radiation (cal cm^{-2} min^{-1}) at earth's surface for various sky conditions. See text for definitions.

Model		R	C	R+C
CMA	0.3332	0.2979	0.2142	0.1915
LHA	0.3114	0.2802	0.1881	0.1716
DHA	0.2655	0.2423	0.1414	0.1340

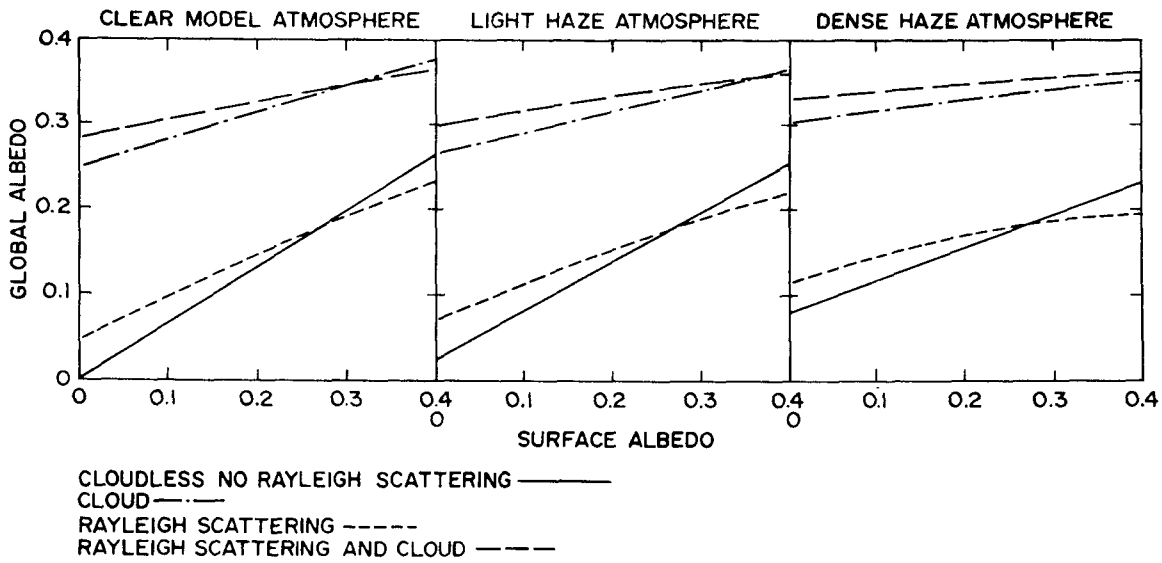

FIG. 4. Global albedo versus surface albedo for various sky conditions.

order of effect as water vapor in the lower troposphere. Because of the presence of large aerosol concentrations near the surface, both the energy which enters into the aerosol layer and the energy reflected back from the surface are trapped in the lower atmosphere, causing larger heating rates. The largest heating rate is found in the first layer for the cloudless DHA. The presence of clouds causes the energy to be scattered back before it can be trapped between the clouds and the surface. Therefore, the tropospheric aerosols have a less pronounced effect in the lower troposphere for cloudy than for cloudless skies.

It is quite clear that, for fixed sky conditions, the effect of an increase of surface albedo is to increase the global albedo, although at a reduced rate because part of the reflected radiation is re-reflected by the aerosols and absorbed in the atmosphere. But, on the other hand, for an arbitrary ground albedo the effect of an increase of atmospheric turbidity is not necessarily to increase the global albedo. We have made calculations with the cloud and aerosol properties fixed but with different ground albedos. In this way we have found the critical surface albedo such that the earth-atmosphere system changes from cooling to heating with the addition of aerosols. Table 6 and Fig. 4 show the global albedo versus surface albedo for cloudless and cloudy skies. It is interesting to note that for a cloudless sky when the surface albedo ρ reaches 0.30, an increase in aerosol decreases the global albedo; the same thing happens when surface albedo is around 0.30 for a cloudy sky. But since the surface albedo on a global scale is around 0.105, the average effect of an increase of atmospheric turbidity is to increase the global albedo, i.e., to cool the earth-atmosphere system.

c. *Infrared radiation*

Table 7 shows the net upward infrared fluxes at the earth's surface and at the top of the atmosphere. Compared with the aerosol-free sky, the LHA reduces the net fluxes at the top and bottom of the atmosphere by 2.4 and 2.3% for a cloudless sky, and by about 1.3 and 2.6% for a cloudy sky; corresponding reductions for the DHA are 4 and 6.5%, and 1.7 and 7.1%.

Table 8 shows the infrared cooling rate based on a temperature profile which has a constant lapse rate

TABLE 5. Solar heating rate $(\partial T/\partial t)_{SW}$ [°K per day] for various sky conditions.

Layer	z (km)	Clear skies			Cloudy skies		
		CMA+R	LHA+R	DHA+R	CMA+R	LHA+R	DHA+R
1	0.08	1.6309	1.9464	2.9537	1.0101	1.3840	1.7579
2	0.64	1.0759	1.3532	2.2444	0.6651	1.0166	1.5669
3	1.71	0.9543	1.1113	1.5500	0.5910	0.8162	1.3108
4	3.27	0.9446	0.9937	1.1058	0.5919	0.6670	0.8318
5	5.37	0.9916	1.0037	1.0046	1.5485	1.5785	1.6014
6	8.10	0.9657	0.9764	0.9660	1.4068	1.4745	1.6331
7	11.80	0.4486	0.4717	0.4594	0.3947	0.4137	0.4043
8	17.74	0.1976	0.2442	0.2316	0.1347	0.1732	0.1636
9	31.24	2.2727	2.2716	2.2495	2.2435	2.2396	2.2182

TABLE 6. Critical surface albedo at which the earth-atmosphere system changes from cooling to heating due to the presence of aerosols.

Surface albedo ρ	Clear skies			Cloudy skies		
	CMA+R	LHA+R	DHA+R	CMA+R	LHA+R	DHA+R
0	0.0475	0.0704	0.1182	0.2841	0.2990	0.3326
0.10	0.0966	0.1123	0.1454	0.3039	0.3143	0.3401
0.20	0.1448	0.1531	0.1702	0.3248	0.3302	0.3475
0.30	0.1911	0.1913	0.1893	0.3465	0.3465	0.3544
0.40	0.2326	0.2225	0.1930	0.3688	0.3629	0.3603

(-6.5K km^{-1}) in the troposphere and a constant temperature (218K) in the stratosphere. Tremendous cooling occurs in the first layer due to the fact that the maximum concentration of water vapor appears very close to the ground and thus much more convection is needed to maintain a stable temperature gradient. The cooling rate increase in layer 7 (below the tropopause) is due mainly to the sudden decrease of water vapor concentration (mixing ratio, 2.0×10^{-6} gm gm^{-1}) in the stratosphere which allows the longwave emission to escape more easily. However, this effect is partially offset by the heating effect of carbon dioxide and ozone in the upper troposphere due to the constant temperature distribution in the stratosphere. A 1K per day difference is observed in the first layer due to dense aerosols as compared to the CMA+R both for cloudless and cloudy skies. Another interesting feature is that the cooling rate decreases by 20–30% in the lower stratosphere even though the aerosol concentration is negligible there. Hence, under radiative equilibrium conditions, the stratosphere is warmer than it would otherwise be due to the presence of tropospheric aerosols.

d. Radiative convective equilibrium

Studies of radiative equilibrium of non-gray atmospheres have been carried out by Yamamoto (1953, 1955), Manabe and Möller (1961) and others. Because it neglects atmospheric motions, the model atmosphere always has a cooler upper troposphere and a higher surface temperature than observed values indicate. Therefore, Manabe and Strickler (1964), and Manabe and Wetherald (1967) have made radiative convective equilibrium computations of the atmosphere as the asymptotic state of an initial value problem. They proposed a simple convective adjustment process to approximate the actual heat transport by atmospheric motions. The procedure used is to make an adjustment to a given critical lapse rate of temperature as soon as the lapse rate tends to exceed the critical rate, thereby permitting a more realistic temperature distribution throughout the atmosphere.

In the present work, the procedures of convective adjustment differ from those quoted above. In the numerical computation the radiative convective equilibrium was approached as follows:

1) The radiative temperature change T_i^{n+1} was calculated from the flux divergence:

$$T_i^{n+1}=T_i^n\left[\left(\frac{\partial T}{\partial t}\right)_{\mathrm{LW}}+\left(\frac{\partial T}{\partial t}\right)_{\mathrm{SW}}\right]^n\Delta t, \qquad (24)$$

where LW and SW denote radiative infrared cooling and solar heating, respectively, n is the iteration step, and i the layer. A forward time scheme is used.

2) Before using the new temperature T_i^{n+1} for flux calculation, the lapse rate is checked against the critical lapse rate γ (a moist adiabatic lapse rate of -6.5K km^{-1}) beginning from the surface [throughout the iteration process, the surface temperature and properties of the gas absorbers are fixed]. If the new temperature distribution is not stable in any given layer, then a convective heat flux equal to

$$E_{ci}=\frac{\gamma\Delta z_i-T_{i-1}^n}{\Delta t}\rho_a c_p\Delta z_i \qquad (25)$$

is required in order to maintain a stable atmosphere, i.e., an atmosphere where

$$\left(\frac{\partial T}{\partial t}\right)_{\mathrm{LW}}+\left(\frac{\partial T}{\partial t}\right)_{\mathrm{SW}}+\left(\frac{\partial T}{\partial t}\right)_{\mathrm{conv.}}=0. \qquad (26)$$

3) At steady state, the layers without convection will be in radiative equilibrium with constant net flux (non-zero, because the surface temperature is not cor-

TABLE 7. Infrared outgoing radiation (cal cm^{-2} min^{-1}) for various sky conditions.

	Clear skies			Cloudy skies		
	CMA+R	LHA+R	DHA+R	CMA+R	LHA+R	DHA+R
Top	0.3617	0.3529	0.3475	0.3142	0.3102	0.3089
Surface	0.1452	0.1419	0.1358	0.0988	0.0962	0.0918

TABLE 8. Infrared cooling rate $(\partial T/\partial t)_{LW}$ [°K per day] for various sky conditions.*

Layer	z (km)	T (°K)	Clear skies			Cloudy skies		
			CMA+R	LHA+R	DHA+R	CMA+R	LHA+R	DHA+R
1	0.08	287.75	9.0346	8.3896	8.0570	8.1938	7.5336	7.1500
2	0.64	285.66	3.0779	2.9135	2.9209	2.2281	2.0611	2.0355
3	1.71	280.29	2.0296	1.9727	1.9827	1.1080	1.0541	1.0501
4	3.27	271.59	1.4584	1.4561	1.4615	0.3985	0.4052	0.4182
5	5.37	259.42	1.0947	1.0961	1.1220	0.5946	0.6547	0.7482
6	8.10	243.24	0.5942	0.6057	0.6229	2.9614	3.0137	3.0487
7	11.80	226.03	0.9150	0.9696	0.9783	0.9465	0.9750	0.9804
8	17.74	218.00	0.3287	0.2228	0.2115	0.3683	0.3050	0.3040
9	31.24	218.00	1.3330	1.2190	1.1947	1.3751	1.3508	1.3467

* Surface (0 km) temperature, 288.0K.

rect), while others will be in radiative convective equilibrium with convection supplied from the surface.

4) The surface temperature is changed and processes 1)–3) are repeated until a steady state is reached and the energy is balanced everywhere.

In the numerical calculations, the initial temperature profile used always obeyed the critical lapse rate in the troposphere and was constant in the stratosphere. At steady state the relative magnitude of the difference between the net outgoing longwave radiation and the net incoming solar radiation is always smaller than 10^{-4} times the incoming solar radiation. At the earth's surface, the excess of net downward solar radiation over net upward longwave radiation is equal to the convection needed in the atmosphere.

Numerical results were obtained for the three atmospheric models CMA, LHA, DHA in radiative convective equilibrium. Table 9 shows the heat balance components of these three models with and without clouds. The theoretical results of Manabe and Strickler (1964), and London (1957) are also given. Slight discrepancies in the results can be attributed to the fact that the various atmospheric models used different gas amounts, transmission functions and cloud conditions, and that calculation of absorption due to Rayleigh scattering was not always included. But, in general, they are quite consistent. The most important point is that in the present model the coupling effects of clouds, surface albedo, Rayleigh and Mie scattering, and non-gray gas absorption are considered by solving the radiative transfer equation approximately, rather than by adding up the individual contributions of those factors.

The resulting temperature and convection distributions are listed in Table 10 and shown in Fig. 5. For a cloudless atmosphere, the surface temperature is 300.84K for CMA and 298.78K for LHA and DHA. Convection is needed for the whole troposphere. As the number density of aerosols increases, convection decreases because the aerosols not only absorb solar energy but also increase the optical path length due to multiple scattering.

In the visible and near infrared, the major effect of the clouds is to increase the heating rate within and above the clouds due to the absorption by water droplets and to the reflection of solar radiation, respectively; the heating rate beneath the clouds is

TABLE 9. Heat balance components (cal cm^{-2} min^{-1}) of the radiative convective atmosphere.*

	CMA+R					LHA+R		DHA+R	
	Cloudless		Clouds						
	Present model	Manabe and Strickler	Present model	Manabe and Strickler	London	Cloudless	Clouds	Cloudless	Clouds
Top of Atmosphere									
longwave	0.4505	0.4287	0.3475	0.3266	0.324	0.4428	0.3424	0.4266	0.3298
shortwave	0.4505	−0.4286	−0.3475	−0.3266	−0.324	−0.4428	−0.3424	−0.4266	−0.3298
Earth's surface									
longwave	0.1352	0.1485	0.0737	0.0854	0.090	0.1392	0.0731	0.1331	0.0492
shortwave	−0.2979	−0.3360	−0.1915	−0.2365	−0.237	−0.2802	−0.1717	−0.2423	−0.1340
Surface temperature	300.840	300.30	287.430	286.9	288.0	298.775	285.200	296.415	276.750
Convection									
$\sum_{i=1}^{N} E_{ci}$	0.1627	0.1875	0.1178	0.1511	0.147	0.1411	0.0986	0.1092	0.0848
Global albedo	0.0990	0.1426	0.3049	0.3468	0.352	0.1144	0.3151	0.1467	0.3405

*Positive values designate upward flux.

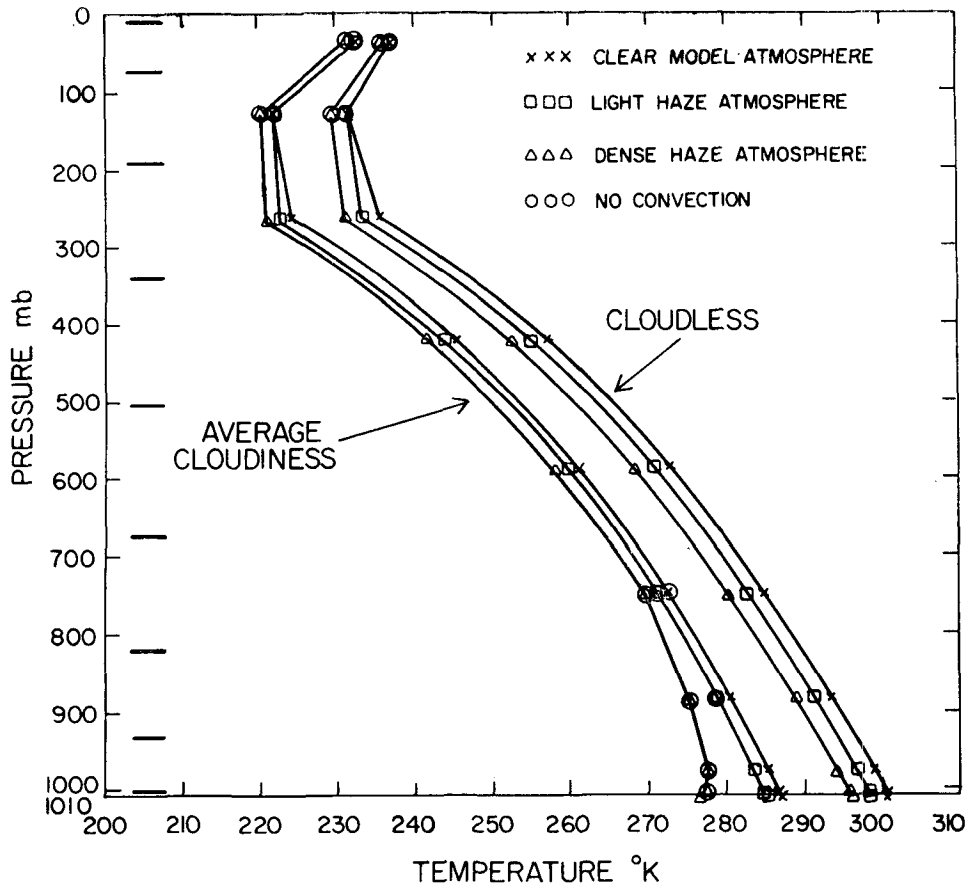

FIG. 5. Radiative convective equilibrium temperature distribution of the earth's atmosphere.

decreased because the solar flux is reduced by the clouds. In the infrared, the clouds are treated as black. Consequently, larger cooling rates appear above the clouds while smaller values are found within and beneath. Therefore, superadiabatic lapse rates are observed beneath the clouds (zero convection) in layer 4 and convection is needed right above cloud layer 5.

For the cloudy atmosphere, CMA+R (considered as the current earth's atmosphere) has a surface temperature of 287.43K which is very close to the present mean global surface temperature of 288K. The lower and upper stratospheric temperatures are 221.86 and 232.31K, respectively. Light haze cools the surface and the atmosphere except for a 0.04K temperature increase at the lower stratosphere; the total convection is reduced by 17%. Dense haze reduces the surface temperature to 276.75K and convection to 0.085 cal cm^{-2} min^{-1}, i.e., a 28% reduction.

Aerosols act to stabilize the atmosphere by either absorbing solar energy or increasing the path length.

TABLE 10. Convection (cal cm^{-2} min^{-1}) and temperature (°K) distribution of the radiative convective equilibrium atmosphere.*

Layer	CMA+R		LHA+R		DHA+R		CMA+R+C**		LHA+R+C**		DHA+R+C**	
	T	Conv.	T	Conv.	T	Conv.	T	Conv.	T	Conv.	T	Conv.
Surface	300.84	1.63E-1	298.77	1.41E-1	296.41	1.09E-1	287.43	1.18E-1	285.20	9.86E-2	276.75	8.48E-2
1	300.68	7.95E-3	298.62	7.58E-3	296.26	5.75E-3	287.27	5.48E-3	285.04	4.77E-3	277.42	0
2	298.89	3.28E-2	296.82	2.99E-2	294.46	1.91E-2	285.48	1.69E-2	283.25	1.15E-2	277.59	0
3	293.69	4.12E-2	291.62	3.70E-2	289.26	2.69E-2	280.28	6.95E-3	278.21	0	275.75	0
4	284.59	2.96E-2	282.52	2.56E-2	280.16	2.06E-2	272.89	0	271.48	0	270.05	0
5	272.89	2.15E-2	270.82	1.81E-2	268.46	1.61E-2	261.19	1.89E-3	259.78	2.12E-3	258.14	1.16E-2
6	257.29	1.53E-2	255.22	1.18E-2	252.86	1.05E-2	245.59	7.57E-2	244.18	7.18E-2	241.58	6.54E-2
7	235.84	1.44E-2	233.77	1.09E-2	231.41	1.01E-2	224.14	1.09E-2	222.73	8.35E-3	221.14	7.77E-3
8	231.87	0	231.62	0	229.73	0	221.86	0	221.90	0	220.66	0
9	237.79	0	237.64	0	236.50	0	232.31	0	232.36	0	231.56	0

* Tabular entries for convection include exponent of 10 factor, i.e., $1.63E\text{-}1 = 1.63 \times 10^{-1}$.
** The clouds appear at the top of layer 5.

TABLE 11. Comparison of present calculations with observations of Vonder Haar and Suomi.

	Global albedo	Infrared loss (cal cm^{-2} min^{-1})
Computed	0.3049	0.3475
Measured	0.30	0.34

More important, however, is the fact that a temperature inversion forms near the surface due to the large aerosol concentration. In other words, particle scattering and absorption eliminate the requirement for convection, and radiation becomes the dominant transfer mechanism.

Recent analysis of long-time satellite measurements of the earth's radiation budget and global albedo by Vonder Haar and Suomi (1971) agrees very well with the present calculations. Table 11 shows the computed and measured values; the differences are within 2–3%.

4. Conclusions

1) The perturbation technique introduced allows approximate solution of the radiative transfer equation in nonhomogeneous media with non-gray gas absorption, Rayleigh scattering, and anisotropic particle scattering. An asymptotic matching process is performed to match the approximate solution to the modified two-flux solution at single-scatter albedos of $a=0$ and $a=1.0$. When $\tau_0=1.0$, the agreement is nearly perfect for all values of a. Even for $\tau_0=10.0$, the approximation is in excellent agreement for $a<0.4$ and $a>0.99$. Applied to the earth's atmosphere, this technique permits use of narrow band models for non-gray gases (H_2O, CO_2, O_3) as well as realistic Rayleigh and Mie scattering coefficients in order to study the effects of aerosols.

2a) It is found that the effects of aerosols in the infrared cannot be neglected. The net flux at the surface is reduced by 2.6% for light haze ($\tau^p_{\lambda=10\,\mu m}=0.01676$, $a^p_{\lambda=10\,\mu m}=0.473$) and as high as 7% for dense haze ($\tau^p_{\lambda=10\,\mu m}=0.0594$). In the visible, light haze ($\tau^p_{\lambda=0.55\,\mu m}=0.223$, $a^p_{\lambda=0.55\,\mu m}=1.0$) and dense haze ($\tau^p_{\lambda=0.55\,\mu m}=0.789$) increase the global albedo from 0.305 to 0.315 and 0.340, respectively.

2b) The combined effects of clouds, aerosols and surface albedo are important in determining whether heating or cooling of the earth-atmosphere system occurs. The model used in these calculation indicates that the increase of atmospheric turbidity (due to aerosol alone) may decrease the global albedo for the case when the surface albedo is larger than 0.30, i.e., heating of the earth-atmosphere due to the presence of aerosol is possible for a high albedo surface such as dry grass land, desert or snow covered ground. For the same reason, the presence of stratospheric aerosols with underlying clouds (high albedo) may also cause heating if higher water vapor concentration is found in the stratosphere.

3) The aerosols reduce the convection needed to maintain a stable atmosphere. For the dense haze model, a temperature inversion develops close to the surface where the required convection is zero, and radiation becomes the dominant heat transfer mechanism.

Acknowledgments. The author would like to thank Dr. S. I. Rasool, who initiated this program. We would also like to thank Dr. J. E. Hansen for his interest and help. The financial support of the National Aeronautics and Space Administration under Grant NGL 33-008-012 is acknowledged. The senior author now holds an NAS–NRC resident research associateship at the Goddard Institute for Space Studies.

REFERENCES

Angstrom, A., 1962: Atmospheric turbidity, global illumination and planetary albedo of the earth. *Tellus*, **14**, 435–450.

Braslau, N., and J. V. Dave, 1973: Effect of aerosols on the transfer of solar energy through realistic model atmospheres, Parts I and II. *J. Appl. Meteor.*, **12**, 601–619.

Canosa, J., and H. R. Penafiel, 1973: A direct solution of the radiative transfer equation: Application to Rayleigh and Mie atmospheres. *J. Quant. Spectros. Radiat. Transfer*, **13**, 21–39.

Chandrasekhar, S., 1960: *Radiative Transfer*. New York, Dover, 393 pp.

Charlson, R. S., and M. J. Pilat, 1969: Climate: The influence of aerosols. *J. Appl. Meteor.*, **8**, 1001–1002.

Chu, C. M., and S. W. Churchill, 1955: Numerical solution of problems in multiple scattering of electromagnetic radiation. *J. Phys. Chem.*, **59**, 855–863.

Conover, J. H., 1965: Cloud and terrestrial albedo determinations from TIROS satellite pictures. *J. Appl. Meteor.*, **4**, 378–386.

Deirmendjian, D., 1964: Scattering and polarization properties of water clouds and hazes in the visible and infrared. *Appl. Opt.*, **3**, 187–196.

Domoto, G. A., and W. C. Wang, 1974: Radiative transfer in homogeneous non-gray gases with non-isotropic particle scattering. *J. Heat Transfer, ASME Trans.*, August.

Edwards, D. K., and W. A. Menard, 1964: Comparison of models for correlation of total band absorption. *Appl. Opt.*, **3**, 621–625.

Elsasser, W. M., and M. F. Culbertson, 1960: Atmospheric radiation tables. *Meteor. Monogr.*, **4**, No. 23.

Elterman, L., 1968: UV, Visible, and IR attenuation for altitudes to 50 km. AFCRL-68-0153.

Goody, R. M., 1964: *Atmospheric Radiation: I. Theoretical Basis*. Oxford University Press, 436 pp.

Grant, I. P., and G. E. Hunt, 1968: Solution of radiative transfer problems in planetary atmospheres. *Icarus*, **9**, 526–534.

Griggs, M., 1968: Aircraft measurements of albedo and absorption of stratus clouds, and surface albedos. *J. Appl. Meteor.*, **7**, 1012–1017.

Handbook of Geophysics, 1961: New York, The Macmillan Co.

Hansen, J. E., 1969: Radiative transfer by doubling very thin layers. *Astrophys. J.*, **155**, 565–573.

Houghton, H. G., 1954: On the annual heat balance of the Northern Hemisphere. *J. Meteor.*, **11**, 1–9.

Irvine, W. M., 1968: Multiple scattering by large particles: II. Optically thick layers. *Astrophys. J.*, **152**, 823–834.

Kattawar, G. W., and G. N. Plass, 1968: Radiance and polarization of multiple scattered light from haze and clouds. *Appl. Opt.*, **7**, 1519–1527.

Krakow, B., H. J. Babrov, G. J. Maclay and A. L. Shabott, 1966: Use of Curtis-Godson approximation in calculation of radiant heating by inhomogeneous hot gases. *Appl. Opt.*, **5**, 1791–1800.

Landsberg, H. E., 1970: Man-made climate changes. *Science*, **170**, 1265–1274.

List, R. M., Ed., 1968: *Smithsonian Meteorological Tables*, 6th ed. Washington, D. C., Smithsonian Institution.

London, J., 1957: A study of the atmospheric heat balance. Final report, Contract AF 19(122)-165, College of Engineering, New York University.

Manabe, S., and F. Möller, 1961: On the radiative equilibrium and heat balance of the atmosphere. *Mon. Wea. Rev.*, **89**, 503–532.

——, and R. F. Strickler, 1964: Thermal equilibrium of the atmosphere with a convective adjustment. *J. Atmos. Sci.*, **21**, 361–385.

——, and R. T. Wetherald, 1967: Thermal equilibrium of the atmosphere with a convective adjustment. *J. Atmos. Sci.*, **24**, 241–259.

Malkmus, W., 1967: Random Lorentz band model with exponential-tailed S^{-1} line intensity distribution function. *J. Opt. Soc. Amer.*, **57**, 323–329.

McClatchey, R. A., R. W. Fenn, J. E. A. Selby, F. E. Volz and J. S. Garing, 1971: Optical properties of the atmosphere (revised). AFCRL-71-0279.

McCormick, R. A., and J. H. Ludwig, 1967: Climate modification by atmospheric aerosols. *Science*, **156**, 1358–1359.

Mitchell, J. M., Jr., 1971: The effect of atmospheric aerosols on climate with special references to temperature near the earth's surface. *J. Appl. Meteor.*, **10**, 703–714.

Neiburger, M., 1949: Reflection absorption, and transmission of insolation by stratus cloud. *J. Meteor.*, **6**, 98–104.

Pitts, E., 1954: The application of radiative transfer theory to scattering effects in unexposed photographic emulsions. *Proc. Phys. Soc. London*, **67**, 105–119.

Plass, G. N., 1963: Spectral band absorptance for atmospheric slant path. *Appl. Opt.*, **2**, 515–526.

Potter, J. F., 1970: The delta function approximation in radiative transfer theory. *J. Atmos. Sci.*, **27**, 943–949.

Rasool, S. I., and S. H. Schneider, 1971: Atmospheric carbon dioxide and aerosols: Effects of large increases on global climate. *Science*, **173**, 138–141.

Robinson, N., 1966: *Solar Radiation*. Amsterdam, Elsevier, 347 pp.

Romanova, L. M., 1962: I. The solution of the radiative transfer equation for the case when the indicatrix of scattering greatly differs from the spherical one. *Opt. Spek.*, **13**, 429–435.

Sagan, C., and J. B. Pollack, 1967: Anisotropic non-conservative scattering and the clouds of Venus. *J. Geophys. Res.*, **72**, 469–477.

Study of Critical Environment Problem (SCEP), 1970: *Man's Impact on the Global Environment*. The MIT Press, 319 pp.

Schuster, A., 1905: Radiation through a foggy atmosphere. *Astrophys. J.*, **21**, 1–22.

Schwarzschild, K., 1906: On the equilibrium of the Sun's atmosphere. *Nachr. Gesell. Wiss. Gottingen, Math.-Phys. Kl.*, **195**, 41–53.

Sellers, W. D., 1965: *Physical Climatology*. The University of Chicago Press, 272 pp.

Smith, W. L., 1966: Note on the relationship between total precipitable water and surface dew point. *J. Appl. Meteor.*, **5**, 726–727.

Tien, C. L., 1968: Thermal radiation properties of gases. *Advances in Heat Transfer*, Vol. 5, New York, Academic Press, 253–324.

Twomey, S., H. Jacobowitz and H. B. Howell, 1966: Matrix methods for multiple-scattering problems. *J. Atmos. Sci.*, **23**, 289–296.

Uesugi, A., and W. M. Irvine, 1969: Computation of synthetic spectra for a semi-infinite atmosphere. *J. Atmos. Sci.*, **26**, 973–978.

van de Hulst, H. C., 1963: A new look at multiple scattering. Goddard Institute for Space Studies, NASA, New York.

——, 1964: Diffuse reflection and transmission by a very thick plane-parallel atmosphere with isotropic scattering. *Icarus*, **3**, 336–341.

——, and K. Grossman, 1968: Multiple light scattering in planetary atmospheres. *The Atmospheres of Venus and Mars*, J. C. Brandt and M. E. McElroy, Eds., New York, Gordon and Breach, 35–55.

Vonder Haar, T. H., and V. E. Suomi, 1971: Measurements of the earth radiation budget from satellites during a five year period. Part I: Extended time and space means. *J. Atmos. Sci.*, **28**, 305–314.

Wang, W. C., 1973: Doctoral dissertation, Columbia University, p. 13.

Yamamoto, G., 1953: Radiative equilibrium of the earth's atmosphere: I. The gray case. *Sci. Rept. Tohoku Univ.*, Ser. 5 (Geophys.), **5**, 45–57.

——, 1955: Radiative equilibrium of the earth's atmosphere: II. The use of Rosseland's and Chandrasekhar's means in the line absorbing case. *Sci. Rept. Tohoku Univ.*, Ser. 5 (Geophys.), **6**, 127–136.

——, and M. Tanaka, 1972: Increase of global albedo due to air pollution. *J. Atmos. Sci.*, **29**, 1405–1412.